

1 **The iron-dopamine D1 coupling modulates neural signatures of**
2 **working memory across adult lifespan**

3 Jonatan Gustavsson¹, Jarkko Johansson², Farshad Falahati¹, Micael Andersson⁴, Goran Papenberg¹,
4 Bárbara Avelar-Pereira¹, Lars Bäckman¹, Grégoria Kalpouzos*¹, Alireza Salami*^{1,3,4}

5 ¹Aging Research Center, Karolinska Institutet and Stockholm University, Sweden. ²Umeå University,
6 Faculty of Medicine, Department of Radiation Sciences, Sweden. ³Wallenberg Center for Molecular
7 Medicine at Umeå University ⁴ Department of Integrative Medical Biology, Umeå University, Umeå,
8 Sweden

9 *Authors share the position as last authors.

10

11 **Abstract**

12 Brain iron overload and decreased integrity of the dopaminergic system have been independently
13 reported as brain substrates of cognitive decline in aging. Dopamine (DA), and iron are co-localized in
14 high concentrations in the striatum and prefrontal cortex (PFC), but follow opposing age-related
15 trajectories across the lifespan. DA contributes to cellular iron homeostasis and the activation of D1-
16 like DA receptors (D1DR) alleviates oxidative stress-induced inflammatory responses, suggesting a
17 mutual interaction between these two fundamental components. Still, a direct in-vivo study testing
18 the iron-D1DR relationship and their interactions on brain function and cognition across the lifespan
19 is rare. Using PET and MRI data from the DyNAMiC study (n=180, age=20-79, %50 female), we
20 showed that elevated iron content was related to lower D1DRs in DLPFC, but not in striatum,
21 suggesting that dopamine-rich regions are less susceptible to elevated iron. Critically, older
22 individuals with elevated iron and lower D1DR exhibited less frontoparietal activations during the
23 most demanding task, which in turn was related to poorer working-memory performance. Together,
24 our findings suggest that the combination of elevated iron load and reduced D1DR contribute to
25 disturbed PFC-related circuits in older age, and thus may be targeted as two modifiable factors for
26 future intervention.

27 **Keywords:** Dopamine, Iron, Working memory, Age, BOLD

28 **Highlights**

29 • First study demonstrating the association between regional iron and dopamine D1DR in adult
30 humans.

31 • The interplay between age-related elevated iron and diminished D1DR explained lower task-
32 related brain activity, which in turn was related to poorer task performance.

33 • Our findings iron-DA coupling can help progress the understanding of the mechanisms
34 behind DA-related neurodegeneration.

35 **1 Introduction**

36 Aging is associated with cognitive decline (Gorbach et al., 2017; Salthouse, 2012) and concomitant
37 alterations in structural, functional, and molecular properties of the brain (Andrews-Hanna et al.,
38 2007; Bäckman et al., 2000; Gorbach et al., 2017; Zimmerman et al., 2006). Elevated iron content and
39 decreased integrity of the dopaminergic system are typically reported as independent brain
40 substrates of age-related cognitive decline (Bäckman et al., 2006, 2011; Cools & D'Esposito, 2011;
41 Daugherty et al., 2015; Gustavsson et al., 2022; Hallgren & Sourander, 1958; Kalpouzos, 2018; Landau
42 et al., 2009; Nyberg, Andersson, et al., 2009; Salami et al., 2019). Intracellular non-heme iron is
43 involved in several fundamental neurobiological processes, including dopamine (DA) metabolism
44 (Hare & Double, 2016; Mills et al., 2010). More specifically, iron is a cofactor of tyrosine hydroxylase
45 during DA synthesis, indicating a critical role of iron in DA metabolism as well as in the development
46 of the dopaminergic system (Erikson et al., 2001; Ortega et al., 2007; Unger et al., 2014; Zucca et al.,
47 2017).

48 Iron is stored in the ferritin protein which keeps it from harming brain cells and is released upon
49 metabolic demand. However, unbound iron accumulates with advancing aging and exerts
50 detrimental effects on cellular integrity. Elevated iron content contributes to poorer myelin integrity
51 (Steiger et al., 2016) and grey-matter atrophy (Daugherty & Raz, 2015, 2016), as well as altered
52 frontostriatal activity (Kalpouzos et al., 2017; Rodriguez et al., 2020; Salami et al., 2021) along with
53 disrupted functional connectivity in aging (Salami et al., 2018). Similar to consequences of elevated
54 iron in aging, disruption of the DA system contributes to age-related neurocognitive impairment
55 (Bäckman et al., 2006, 2011; Cools & D'Esposito, 2011; Landau et al., 2009; Nyberg, Dahlin, et al.,
56 2009; Rieckmann et al., 2011; Salami et al., 2019). Given DA and iron are co-localized in high
57 concentrations in the striatum, age-related iron dyshomeostasis combined with disturbance of the
58 DA system may become harmful for brain integrity and cognition. Direct in-vivo studies testing the

59 synergistic effects between the dopaminergic system and iron on brain function and cognition in
60 aging are rare.

61 Past studies suggest that iron may cause neurotoxicity through DA oxidation, which may in turn
62 contribute to loss of dopaminergic neurons (Hald & Lotharius, 2005; Hare & Double, 2016; Youdim et
63 al., 1993; Zucca et al., 2017). Animal studies have demonstrated that iron-induced damage causing
64 DA depletion (Poetini et al., 2018) and deterioration of dopaminergic cells (Kaur et al., 2003) could be
65 restored after iron chelation. In contrast, a longitudinal study showed that dopaminergic cell death
66 precedes iron elevation in parkinsonian monkey (He et al., 2003). A study with young, middle-aged,
67 and older rhesus monkeys reported an association between iron and stimulus-evoked levels of DA
68 (Cass et al., 2007), with older monkeys exhibiting more iron accumulation and less DA release.
69 Although it remains unclear whether elevated iron is the cause or consequence of DA degeneration,
70 it is relatively well acknowledged in animal studies that these two key chemical components of the
71 brain interact with each other (Hare & Double, 2016).

72 As opposed to ample animal studies on iron-DA coupling, evidence for such an association across the
73 adult lifespan in humans is scarce. A recent longitudinal study showed that developmental changes in
74 pre-synaptic, but not post-synaptic, DA receptors were positively associated with iron accumulation
75 through adolescence and young adulthood (Larsen et al., 2020). Still, iron and DA play ambivalent
76 roles during early and later adulthood (Johansson et al., 2022; Kalpouzos et al., 2017; Salami et al.,
77 2021). Recent work showed that older individuals with genetic predisposition for lower DA (by proxy
78 of the *COMT* Val158Met genetic polymorphism) accumulated more iron in the dorsolateral
79 prefrontal cortex (DLPFC) and striatum over 3 years (Gustavsson et al., 2022). Postsynaptic DA
80 markers, particularly DA D1-like receptor (D1DRs) which are the most abundantly expressed receptor
81 subtypes, are among the most age-sensitive DA systems (Karrer et al., 2019). Moreover, the
82 activation of D1 and D2 receptors alleviates oxidative stress-induced inflammatory responses (Shao
83 et al., 2013; Yan et al., 2015; Zhu et al., 2018). Hence, with diminished DADRs, the capacity of the

84 protective response counteracting oxidative stress and neuroinflammation due to iron overload is
85 lessened, and may lead to increased damage and ferroptosis (Hald & Lotharius, 2005).

86 Motivated by the lack of human studies, we investigated the relationship between dopaminergic
87 receptors and iron content, and their interactions on brain function and cognition. Using the largest
88 D1DR dataset across the world, we studied 180 healthy individuals (20-79 years old) who underwent
89 D1DR Positron Emission Tomography (PET) assessment using [¹¹C]SCH23390, iron approximation
90 made with magnetic resonance imaging (MRI) based quantitative susceptibility mapping (QSM;
91 (Langkammer et al., 2012)), and functional magnetic resonance imaging (fMRI) while performing a
92 working-memory task. We first examined regional variation in the link between D1DR and iron
93 content with the hypothesis that greater iron content is related to lower D1DR, with a possible
94 interaction with age (C.f. Salami et al., 2021; Kalpouzos et al., 2018). We targeted DLPFC and striatum,
95 because of abundantly expressed D1DR (Shohamy & Adcock, 2010), pronounced age-related D1DR
96 differences (Karrer et al., 2017), and association between *COMT* polymorphism (i.e., a dopaminergic
97 gene) and iron accumulation reported in these regions (Gustavsson et al., 2022). Given the
98 association of iron and DA to neural circuits of working memory (c.f., Salami et al., 2021; Salami et al.,
99 2019), we predicted an interactive effect of iron and D1DR on load-dependent BOLD modulation and
100 working memory processing (Gustavsson et al., 2022; Spence et al., 2020). To this end, we applied
101 multivariate partial-least squares (PLS; ((McIntosh & Lobaugh, 2004)) which enables a simultaneous
102 analysis of iron content, D1DR, age, on BOLD associations across all task conditions in a data-driven
103 fashion. If these variables are simultaneously related to neural circuits of WM, PLS should reveal a
104 single network showing that older individuals with elevated iron and decreased D1DR (i.e., toxic iron-
105 DA coupling) exhibit lower task-related BOLD-response, particularly within the frontoparietal
106 network. However, if D1DR and iron differentially modulate BOLD response (c.f., Salami et al., 2019;
107 Salami et al., 2021), PLS should reveal different networks.

108 **2 Materials and methods**

109 This study uses data from the DopamiNe Age Connectome Cognition (DyNAMiC) project approved by
110 the Umeå University Regional Ethical Board. All participants signed informed consent prior to data
111 collection (for details about DyNAMiC, see Nordin et al., 2022).

112 **2.1 Participants**

113 One-hundred and eighty adults (mean age 49.8 ± 17.4 years; range 20-79; 90 females) from Umeå,
114 Sweden, were recruited to participate in the project and underwent the full protocol, including
115 cognitive testing, MRI, and PET assessments. All participants were native Swedish speakers, right-
116 handed, and had no history of neurological illnesses. Of the sample of 180 participants, 3 dropped
117 out of PET scanning, 4 were excluded due to incidental brain abnormalities, 3 due to failed
118 reconstruction of QSM images. Additionally, brain and behavioural data were screened for univariate
119 and multivariate outliers. Univariate outliers were defined as values greater or less than 3.29 SD from
120 the mean (Tabachnick & Fidell, 2013) and excluded as pairwise deletions per ROIs and modality.
121 Multivariate outliers were identified according to Mahalanobis distance ($p < 0.001$; Tabachnick &
122 Fidell, 2013). As a result, five participants were identified as univariate outliers on their iron ($n=3$) or
123 D1DR ($n=2$) values, and three were multivariate outliers. Thus, data from 162 individuals were used
124 in the analyses involving iron content and D1D1R. Furthermore, three outliers were identified based
125 on their online WM performance and excluded from analyses.

126 **2.2 Neuroimaging acquisition and pre-processing**

127 Participants underwent positron emission tomography on a Discovery 690 PET/CT scanner (General
128 Electric) and MRI on a Discovery MR750 3.0 T scanner (General Electric) equipped with a 32-channel
129 phased-array head coil at two separate occasions at Umeå University Hospital.

130 **2.2.1 PET acquisition**

131 PET was conducted to assess whole-brain D1DR using radioligand [^{11}C]SCH23390 at rest (for details
132 see Nordin et al., 2022). The scanning session started with a low-dose CT image, followed by an

133 intravenous bolus injection of the radioligand. Participants were instructed to lay still and stay awake
134 with eyes open. An individually fitted thermoplastic mask was attached to the bed surface during
135 scanning to minimize head movement.

136 **2.2.2 Structural MR acquisition**

137 High-resolution anatomical T1-weighted images were acquired using 3D fast-spoiled gradient echo
138 sequence with the following parameters: 176 sagittal slices, slice thickness = 1 mm, voxel size 0.49 x
139 0.49 x 1 mm³, repetition time (TR) = 8.2 ms, echo time (TE) = 3.2 ms, flip angle = 12°, field of view
140 (FOV) = 250 x 250 mm, no spacing.

141 **2.2.3 Iron acquisition**

142 Images for iron estimation was obtained using a 3D multi-echo gradient-recalled echo sequence
143 (meGRE). The parameters were as follows: 124 axial slices, voxel size 1 x 1 x 1.2 mm³, TR = 31 ms, flip
144 angle = 17°, FOV = 256 x 256 mm, no spacing. The first TE was 1.78 ms followed by seven additional
145 TEs with a 2.87 ms interval.

146 **2.2.4 Functional MR acquisition**

147 The functional images were sampled using single-shot multiband EPI sequence with 37 axial slices,
148 voxel size 1.95 x 1.95 x 3.9 mm³, 0.5 mm spacing, TR = 2.000 ms, TE = 30 ms, flip angle = 80°, and FOV
149 = 250 x 250 mm. Ten dummy scans were collected at the start of the sequence.

150 **2.2.5 In-scanner working memory task**

151 A numerical N-back task was administered in the scanner (Salami et al., 2018). A sequence of single
152 numbers appeared on the screen for 1.5s, with an interstimulus interval of 0.5s. During every item
153 presentation, subjects indicated whether the digit on the screen was the same as the one shown 1, 2,
154 or 3 digits back by pressing one of the two adjacent buttons with the index (Yes response) or middle
155 finger (No response). Each working-memory load condition (1-, 2-, and 3-back) was presented over
156 nine blocks in random order (interblock interval, 22 s) with each block consisting of 10 trials. For

157 every block, 10 trials were performed with four matches (requiring a “yes” response) and six
158 nonmatches (requiring a “no” response). The N-back blocks were counterbalanced and trial sequence
159 was the same for all participants. The maximum score for each condition was 81, 72, 63, respectively.
160 Performance was calculated as an error-adjusted discrimination score by subtracting the proportion
161 of false alarms (i.e., a wrong answer judged to be correct, or, in other terms, answering Yes, when
162 the correct answer is No) from the proportion of correct hits (i.e., answering Yes when the correct
163 answer is Yes).

164 **2.2.6 PET processing**

165 PET data obtained with [¹¹C]SCH23390 was processed with the following steps: To estimate receptor
166 availability (i.e., D₁DR) in targeted regions, binding potential relative to non-displaceable binding in a
167 reference region (BP_{ND}; Innis et al., 2007) was used with cerebellum as reference. The processing of
168 the PET data included correction for head movement by using frame-to-frame image co-registration,
169 and co-registered with T1-weighted MRI data with re-slicing to MRI voxel size using Statistical
170 Parametric Mapping (SPM12: Wellcome Trust Centre for Neuroimaging,
171 <http://www.fil.ion.ucl.ac.uk/spm/>). To model the regional time-activity course (TAC) data we used
172 simplified reference tissue model (SRTM; Lammertsma & Hume, 1996).

173 **2.2.7 MRI processing**

174 *Quantitative susceptibility mapping.* Processing of QSM is referred from Gustavsson et al. (2022).
175 Approximation of iron content was inferred from susceptibility values derived from QSM images.
176 Morphology-enabled dipole inversion (MEDI; T. Liu et al., 2011) is a method for QSM estimation that
177 selects the solution that minimizes the discrepancy in the number of voxels belonging to edges
178 between the susceptibility image and the magnitude image. Here, we used the recommended
179 nonlinear variant of MEDI proposed by Liu et al. (2013). Initially, the total field map was estimated
180 from the complex meGRE images by performing a nonlinear least square fitting on a voxel-by-voxel
181 basis. The resulting frequency map was then spatially unwrapped using a guided region-growing

182 unwrapping algorithm (Xu & Cumming, 1999). The background fields, the superimposed field
183 contributions that are not caused by the sources inside the brain and mainly generated by air-tissue
184 interference, were eliminated using a nonparametric technique based on Projection onto Dipole
185 Fields (PDF: Liu et al., 2011). Finally, the corrected frequency map was used as input for the field-to-
186 source inverse problem to calculate susceptibility maps. The MEDI Toolbox
187 (<http://weill.cornell.edu/mri/pages/qsm.html>) was used to calculate QSM images.

188 Due to the singularity of dipole kernel at the centre of k-space, the generated QSM images contain
189 relative susceptibility values, which may not necessarily be comparable across subjects. To address
190 this issue, a region of the corticospinal tract was selected as a zero-reference region due to its
191 resilience to age-related degeneration (de Groot et al., 2015) and stable susceptibility across
192 adulthood (Li et al., 2014). Using white-matter areas as reference regions has previously been
193 recommended due to their low standard deviations of susceptibility, indicating low inter-subject
194 variation similar (Straub et al., 2017) or even lower than CSF (Deistung et al., 2013). The process of
195 zero-referencing is described in detail by Garzón and colleagues (2017).

196 Automated segmentation of cortical and deep gray-matter structures was performed with the
197 Freesurfer image analysis suite — version 6 (<http://surfer.nmr.mgh.harvard.edu/>) using T1-weighted
198 images (Fischl et al., 2002; Fischl, Salat, et al., 2004; Fischl, Van Der Kouwe, et al., 2004).

199 Next, QSM and the segmentation results were resampled to the native structural space. Then,
200 statistics including average and standard deviation were computed on the QSM maps. We merged
201 segmented rostral and caudal middle frontal regions from the left and right hemispheres to form
202 DLPFC (Fig. 1A), and the left and right caudate and putamen to form striatum (supplementary
203 materials Fig. 1A).

204 Prior to computing statistics on the QSM maps, the boundary of segmentations was eroded by one
205 voxel, and a fraction (15%) of the most extreme values was removed to avoid the influence of high
206 signal from neighbouring vessels and obtain more robust estimates (Garzón et al., 2017).

207 **2.2.8 Functional MRI processing**

208 Pre-processing of the fMRI data, performed in SPM12 software, included slice-timing correction and
209 motion correction by unwarping and re-alignment to the first image of each volume. The fMRI
210 volumes were then normalized to a sample-specific template generated using Diffeomorphic
211 Anatomical Registration using Exponentiated Lie algebra (DARTEL: Ashburner, 2007), affine
212 alignment to MNI standard space, and spatial smoothing with a 6-mm full width at half maximum
213 (FWHM) Gaussian kernel (voxel size = $2 \times 2 \times 2 \text{ mm}^3$).

214 The pre-processed fMRI data were analysed with spatiotemporal PLS (McIntosh et al., 2004;
215 McIntosh & Lobaugh, 2004) to assess the BOLD association with iron, D1DR, and age across the three
216 experimental WM conditions (1-, 2-, and 3-back). PLS determines time-varying distributed patterns of
217 neural activity as a function of experimental variables (1-, 2-, and 3-back) and regional iron and
218 D1DR. This technique allows for the identification of patterns/networks, which reflect association
219 changes across all regions of the brain simultaneously, rather than assemblies of independent
220 regions, thus ruling out the need for multiple-comparison correction. A detailed description of
221 spatiotemporal PLS analysis for fMRI data has been given in previous reports (Garrett et al., 2010;
222 Grady & Garrett, 2014; Salami et al., 2010, 2012, 2014).

223 The onset of each stimulus within each block of images (1-, 2-, and 3-back) was averaged across
224 blocks for each condition. A cross-block correlation matrix was computed as the correlation between
225 neural activity across experimental conditions (1-, 2-, and 3-back) and variables of interest (age,
226 D1DR, iron) across different regions. Then, the correlation matrix was decomposed using singular
227 value decomposition (SVD), to identify a set of orthogonal latent variables (LVs) representing linear
228 combinations of the original variables:

229 $\text{SVD}_{\text{CORR}} = \text{USV}^T$

230 This decomposition produces a left singular vector of regional susceptibility weights (U), a right
231 singular vector of BOLD weights (V), and a diagonal matrix of singular values (S). This analysis

232 produces orthogonal LVs that optimally represent relations between the variables of interest (age,
233 D1DR, iron) and BOLD. Note that PLS is not mathematically susceptible to collinearity similar to the
234 multiple regression approach (Leibovitch et al., 1999). Each LV contains a spatial pattern exhibiting
235 the brain regions whose activity shows the strongest simultaneous relations to the input variables. To
236 obtain a summary measure of each participant's expression of a particular LV pattern, subject-
237 specific "brain scores" are computed by multiplying each voxel's (i) weight (V) from each LV (j) by the
238 BOLD value in that voxel for person (m), and summing over all (n) brain voxels:

$$\sum_{i=1}^n v_{ij} \text{BOLD}_{im}$$

239

240 Taken together, a brain score represents the degree to which each subject contributes to the
241 multivariate spatial pattern captured by a latent variable.

242 The statistical significance of each LV was assessed using permutation testing. This procedure
243 involved reshuffling the rows of the data matrix and recalculating the LVs of the reshuffled matrix
244 using the same SVD approach. The number of times a permuted singular value exceeds the original
245 singular value yields the probability of significance of the original LV (McIntosh et al., 1996). In the
246 present study, 1000 permutations were performed. In addition, the stability of voxel saliences
247 contributing to each LV was determined with bootstrap estimation of standard errors (SEs), using
248 1000 bootstrap samples (Efron & Tibshirani, 1986). The Bootstrap Ratio (BSR: the ratio between
249 voxel saliences and estimated SEs) was computed and voxels with BSR > 3.29 (similar to a Z-score of
250 3.29, corresponding to $p = 0.001$) were considered reliable. All reliable clusters comprised contiguous
251 voxels, with a distance between clusters of at least 10 mm. Moreover, the upper and lower
252 percentiles of the bootstrap distribution were used to generate 95% confidence intervals (CIs)
253 around the correlation scores to facilitate interpretation (McIntosh & Lobaugh, 2004). For instance, a
254 significant difference between correlation scores in different conditions is indicated by non-

255 overlapping CIs. Similarly, brain or correlation scores were considered unreliable when CIs
256 overlapped with zero.

257 PLS uses all conditions of an experiment and variables of interest at once, thus offering an additional
258 dimension by simultaneously considering both similarities and differences across the experimental
259 variables. If the variables of interest (i.e., age, iron content, D1DR) are similarly related to brain
260 regions, PLS reveals a pattern with reliable loadings (with/without quantitative differences) for all
261 variables. If a single variable dominates the pattern, PLS should reveal a reliable loading for that
262 variable only. Alternatively, if different variables (e.g., D1DR and iron) differentially modulate BOLD
263 response (e.g., Load-dependent effects of dopamine on BOLD as shown in Salami et al., (2019) versus
264 load-independent effect of iron on BOLD shown in Salami et al., 2021), PLS may reveal two distinctive
265 networks.

266 **2.3 Additional statistical analyses**

267 To assess age-effects on cognitive performance, a multivariate analysis of covariance (MANCOVA)
268 was conducted with WM load-conditions as dependent variables and age-groups (younger (age 20-
269 39) vs. middle-aged (age 40-59) vs. older (age 60-79)) as between-subjects factors. Follow-up
270 independent t-tests were conducted to assess significant differences between age groups. To assess
271 the relationship between iron content and D1DR, we conducted partial correlation analyses for each
272 region of interest with iron content and D1DR as dependent variables, controlling for age. As control
273 analyses, we performed the same analyses but included sex, education, and regional grey-matter
274 volume as covariates.

275 **3. Results**

276 **3.1 Demographics**

277 Demographic information along with data on body mass index (BMI), brain volumes, D1DR, and N-
278 back performance are presented in Table 1.

279

280	Table 1. Participant characteristics		
		Mean	SD
281	N (Women)	162 (79)	
	Age	50	17
282	Age range	20-78	
	MMSE	28.8	1.1
283	BMI	25.2	3.9
	Education	15	3.4
	Volume ^a		
284	DLPFC	20478	2696
	Striatum	11473	1282
285	Iron ^b		
	DLPFC	0.0430	0.0140
	Striatum	0.0998	0.0286
286	D1DR		
	DLPFC	0.3582	0.0690
287	Striatum	1.6130	0.2182
	WM performance		
288	1-back accuracy ^c	75.18	6.65
	1-back (H-FA) ^d	0.86	
289	2-back accuracy	60.99	8.77
	2-back (H-FA)	0.72	
290	3-back accuracy	48.10	9.57
	3-back (H-FA)	0.59	

291 *Note. MMSE = Mini Mental State Examination,*
292 *DLPFC = Dorsolateral prefrontal cortex, SD = Standard deviation.*

293 ^a Volume (mL) adjusted for total intracranial volume
294 ^b Approximation of iron, based on susceptibility in parts per million
295 ^c Accuracy calculated as the sum of correct responses
296 ^d Proportion of false alarms (FA) subtracted from proportion of hits
297 (H)

298 The MANCOVA
299 conducted on N-Back performance showed a significant main effect on load conditions ($F_{2,155} =$
300 228.24, $p < 0.001$, Wilk's $\Lambda = 0.253$, partial $\eta^2 = 0.747$), and an age-group effect on load conditions
301 ($F_{4,310} = 9.43$, $p < 0.001$, Wilk's $\Lambda = 0.795$, partial $\eta^2 = 0.108$). Post-hoc analysis for the lowest WM load
302 (1-back) showed that the older participants performed less accurately compared to both middle-
303 aged ($t_{89} = -3.974$, $p < 0.001$) and younger participants ($t_{71} = -5.707$, $p < 0.001$). There was no
304 significant difference between younger and middle-aged participants ($p = 0.07$). For 2-back, older
305 participants performed significantly poorer compared to both middle-aged ($t_{105} = -4.015$, $p < 0.001$)

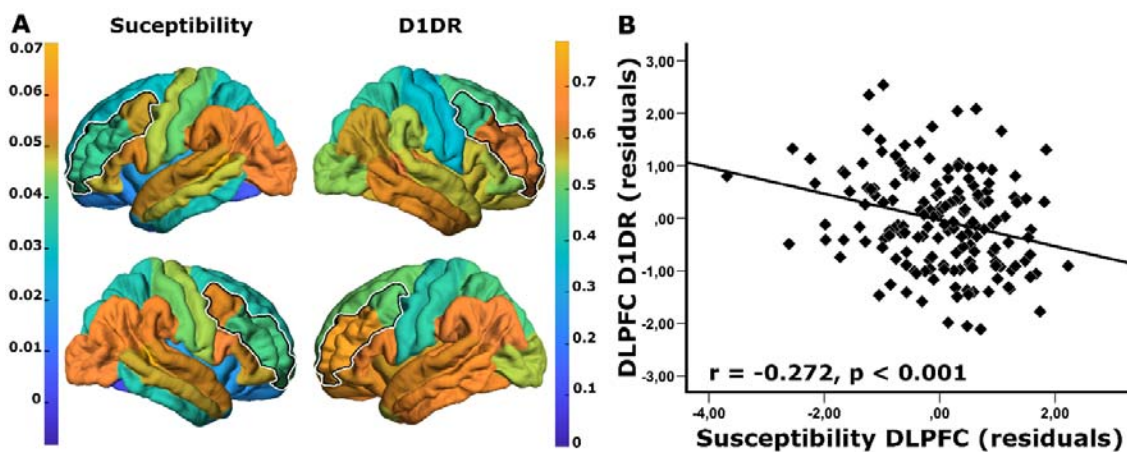
302 and younger participants ($t_{85} = -8.905$, $p < 0.001$). Middle-aged participants performed significantly
303 poorer compared to younger participants ($t_{98} = -4.176$, $p < 0.001$). Lastly, for highest WM load (3-
304 back), older participants performed significantly poorer compared to both middle-aged ($t_{105} = -5.300$
305 $p < 0.001$) and younger participants ($t_{102} = -7.950$, $p < 0.001$). Middle-aged participants performed
306 significantly poorer compared to younger participants ($t_{105} = -2.921$, $p = 0.004$).

307 **3.2 Iron content in DLPFC, but not in striatum, was negatively associated with D1DR**

308 Both striatal and DLPFC iron increased with advancing age (striatum: $r = 0.551$, $p < 0.001$; DLPFC: $r =$
309 0.244 , $p = 0.002$). D1DRs in both regions decreased with advancing age (striatum: $r = -0.62$, $p < 0.001$;
310 DLPFC: $r = -0.565$, $p = < 0.001$).

311 The partial correlation analysis for iron content and D1DR in DLPFC showed a significant negative
312 association across the whole sample ($r = -0.272$, $p < 0.001$), suggesting that greater iron content was
313 linked to lower D1DR (Fig. 1B). Further group level analyses revealed that this correlation was
314 similarly expressed across different age groups (Younger: $r = -0.10$, $p = 0.48$; Middle-aged: $r = -0.30$, p
315 $= 0.026$; Older: $r = -0.37$, $p = 0.006$). However, striatal iron content was unrelated to D1DR across the
316 whole sample ($r = -0.101$, $p = 0.20$; supplementary materials, Fig. 1B). No significant association was
317 observed within each age groups ($P_s > 0.05$), except for a trend-level link in the older individuals ($r = -$
318 0.24 , $p = 0.08$).

319



320

321 **Figure 1.** The relationship between iron content and D1DR in dorsolateral prefrontal cortex. **(A)**
322 Surface map representing distribution of cortical iron (susceptibility in parts per million; left column)
323 and D1DR ($[^{11}\text{C}]\text{SCH23390 BP}_{\text{ND}}$; right column) with dorsolateral prefrontal cortex (DLPFC) outlined.
324 **(B)** Scatterplot depicting the association between greater iron content and lower D1DR in DLPFC. All
325 values are z-transformed residuals adjusting for age.

326

327 **3.3 Iron-D1DR couplings in DLPFC modulates WM-related BOLD in a load-dependent fashion**

328 Given the iron-D1DR link in DLPFC, we next investigated whether iron-D1DR coupling modulated
329 neural correlates of PFC-related function across the adult lifespan. We used behavioural PLS to assess
330 the presence of multivariate spatial patterns of task-related BOLD response dependent on age, iron
331 content, and D1DR across load conditions during N-back working memory task. The analysis
332 identified two significant latent variables (LVs). LV1 represented a brain-wide network with increased
333 activation in older individuals in a load-independent fashion. This network was largely unrelated to
334 D1DR or iron in DLPFC (supplementary materials 5.1.2, Table 1, Fig 2).

335 The second LV represented the canonical WM network (c.f. Nagel et al., 2009; Salami et al., 2018).
336 This LV (permuted $p = 0.02$, 17.97% of cross-block covariance: Fig. 3A) demonstrated that older
337 individuals with elevated iron content and lower D1DR in DLPFC exhibited lower BOLD response in
338 the frontoparietal network during 3-back (Fig. 3B). In contrast, higher BOLD response in the

339 frontoparietal network during 1-back was associated with older age and lower D1DR in DLPFC, but
340 not with iron content. For 2-back, no associations were considered reliable as the CIs overlapped
341 with zero (Fig. 3B). As opposed to the frontoparietal WM network, the default-mode network (Fig. 3A
342 (Blue areas); supplementary Table 2) was less deactivated during 3-back in older individuals with
343 higher iron content and lower D1DR in DLPFC. Taken together, these results revealed that iron-D1DR
344 coupling modulates neural correlates of the working memory in a load-dependent fashion.

345

346

347

348

349

350

351

352

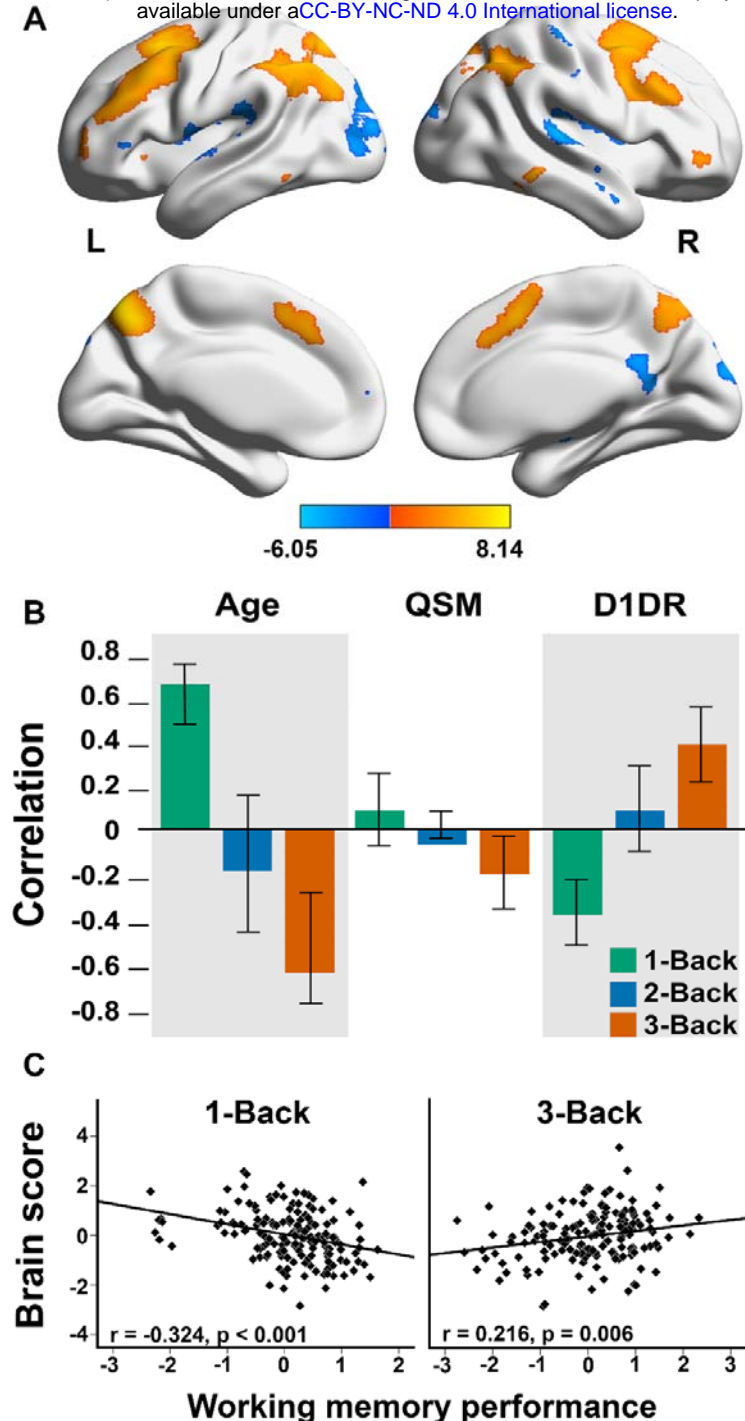
353

354

355

356

357



358 **Figure 3.** Multivariate relationship of BOLD response patterns during working-memory task identified
359 by task PLS. **A)** The regions depicted in a yellow colour mainly correspond to the frontoparietal
360 network, whereas the blue colour mainly represents the default-mode network. The frontoparietal
361 network showed greater activation in correspondence to the behavioural measures across different
362 task conditions, whereas the default-mode network showed greater deactivation (i.e., less
363 activation). **B)** BOLD association across age, iron content (QSM), and D1DR. Interpretation of the
364 figure should be as reliable positive and negative associations of activation (BOLD response) when
365 the confidence intervals (CIs) do not overlap with zero. As the frontoparietal network displayed
366 increased activation, a positive association is interpreted as greater activation, whereas a negative

367 association is interpreted as less activation. For the default-mode network the opposite applies. **C**
368 Greater activation was associated with poorer performance during 1-back, but greater performance
369 during 3-back. All values are z-transformed residuals adjusting for age.

370 **3.4 Load-dependent BOLD response is differentially associated with task performance.**

371 We have shown that increasing age was concomitant with increased and decreased activations
372 within the frontoparietal network during 1-back and 3-back, respectively. We next tested the
373 relationship of brain activation in relation to task performance. The brain score during 1-back was
374 negatively associated with 1-back performance ($r = -0.324$, $p < 0.001$; Fig. 3C), but positively with 3-
375 back ($r = 0.216$, $p = 0.006$; Fig. 3C). No significant association was observed during 2-back ($r = 0.05$,
376 $p=0.4$). Taken together, our results suggest that less frontoparietal activity during 3-back as well as
377 greater frontoparietal activity during 1-back are associated with less efficient working memory
378 function.

379 **3.5 Control analyses**

380 To confirm that the results obtained from the partial correlation analyses were not due to
381 confounding variables, we performed additional analyses in which we controlled for sex, education,
382 and regional grey-matter volume. The inclusion of the additional variables did not result in a
383 noticeable change of the outcome and all the patterns remained consistent. A full description of the
384 results is given in the supplementary results.

385 **4. Discussion**

386 In this study, we provide first in-vivo evidence for an association between D1DR and brain iron across
387 the adult lifespan, and how iron-D1DR synergy may contribute to disturbed brain responses during
388 WM task performance across the lifespan. The main findings were that greater iron content was
389 associated with lower D1DR in DLPFC, but not in striatum, across the adult lifespan. We also found
390 that older individuals with elevated iron content and lower D1DR in DLPFC – a presumably
391 deleterious synergy – exhibited lower frontoparietal activity along with less deactivation of the DMN

392 during high demand condition and in turn poorer WM performance. Although the associations
393 revealed by these data are cross-sectional, a plausible interpretation is that elevated iron and lower
394 D1DR together form a toxic couple (c.f. Hare & Double, 2016), which would contribute to reduced
395 network dynamics and impaired WM processing.

396 A key finding of the present study is the association between higher iron content and lower D1DR in
397 DLPFC across the adult lifespan. The exact mechanism underlying the association between iron
398 content and DA receptors is poorly understood. The dopaminergic system is important to cellular
399 iron homeostasis, as documented in *in vitro* studies (Dichtl et al., 2018; Liu et al., 2021). Supporting
400 this idea, we recently demonstrated that older adults with genetic predisposition for lower DA levels
401 accumulated more iron in DLPFC and striatum over time compared to individuals with presumably
402 higher DA levels (Gustavsson et al., 2022). Age-related differences in pre- and postsynaptic DA
403 markers (Bäckman et al., 2006, 2010) may also contribute to iron dyshomeostasis in aging, resulting
404 in disruption of transportation of iron via transferrin and storage in the ferritin protein (Ward et al.,
405 2014). Disruption of iron handling may lead to increase of ferrous iron, which triggers oxidative
406 stress, neuroinflammation, and cell loss due to ferroptosis (Daugherty et al., 2015; Mazhar et al.,
407 2021; Salami et al., 2021). The activation of D1 and D2/3 receptors alleviates oxidative stress-induced
408 inflammatory responses (Shao et al., 2013; Yan et al., 2015; Zhu et al., 2018). However, whether age-
409 related loss of DA receptors leads to an iron-related increase of oxidative stress and ferroptosis, or
410 whether an age-related increase of iron causes loss of DA receptor cells can only be determined in a
411 longitudinal setting.

412 We did not observe any significant association between iron and D1DR in striatum, except for a
413 trend-level negative association in older age. The reason for these regional variations is unclear. One
414 possibility is that, as D1DR are more expressed in striatum compared to cortex (Shohamy & Adcock,
415 2010), striatal regions are less vulnerable or better at attenuating the damage from higher iron
416 content. If too many receptors diminishes, or the threshold of the capacity for dealing with oxidative

417 stress is exceeded, the iron-induced damage to the cells may lead to ferroptosis (Lillig et al., 2008).
418 This concords well with Parkinson's Disease studies reporting regional variations in synuclein
419 pathology despite brain-wide iron accumulation (McCann et al., 2016), suggesting that additional
420 factors may contribute to iron serving a pathological role.

421 The multivariate PLS analysis revealed that in older age the combination of higher iron and lower
422 D1DR within DLPFC was related to high frontoparietal recruitment during low-demanding tasks along
423 with weak frontoparietal upregulation at higher task demand, which in turn was associated with
424 poorer working memory performance. These results concord with the Compensation-Related
425 Utilization of Neural Circuits Hypothesis (CRUNCH; (Cappell et al., 2010; Mattay et al., 2006; Nyberg
426 et al., 2014; Reuter-Lorenz & Cappell, 2008; Schneider-Garces et al., 2010)), which postulates that
427 neural activity increases at low demanding task-levels in older adults compared to younger adults,
428 but is reduced at more demanding levels.

429 The unique and shared contributions of iron content and neuroinflammation to astrocytic
430 dysfunction in the neurovascular coupling has been proposed to account for the reduced BOLD
431 response (Kalpouzos et al., 2017; Salami et al., 2018, 2021). Higher iron content has been related to
432 inflammation (Haider, 2015; Salami et al., 2021), which can be detrimental to cells during prolonged
433 periods (Hald & Lotharius, 2005; Zecca et al., 2004), thus contributing to astrocytic dysfunction. In
434 vitro studies have demonstrated that DA receptors activation may alleviate and suppress
435 neuroinflammation (Liu et al., 2021; Shao et al., 2013; Yan et al., 2015). A more efficient
436 dopaminergic system (e.g., manifested by greater receptor availability) protect against negative
437 effects of iron and neuroinflammation on brain function. In support of this notion, a past study
438 showed that age-related D1DR alteration alone may contribute to less efficient engagement of
439 working memory circuits (Bäckman et al., 2011). Relatedly, the importance of DA for the
440 frontoparietal BOLD response has been further demonstrated through pharmacological
441 administration of a dopaminergic antagonist, leading to poorer working-memory performance

442 (Fischer et al., 2010). Our results add novel contribution to the previous work, by showing that the
443 combination of elevated iron and D1DR reduction in DLPFC in aging, possibly reflecting synergistic
444 iron-D1DR effects, exerts a deleterious effect in neural circuits of WM. Furthermore, during the most
445 demanding WM condition (3-back), lower activation in the frontoparietal network was related to
446 worse performance, in concordance with previous reports (Salami et al., 2021). Longitudinal data are
447 needed to identify the primary mechanism of disturbed working memory circuit in older age.

448 Our study is the first to link regional iron content to DA receptor availability, by showing that greater
449 iron content is related to lower D1DR. Critically, an interplay between age-related elevated iron
450 content and diminished D1 receptor availability may provide a mechanistic understanding of how
451 iron-DA coupling may exert deleterious effects on neural function and ultimately cognition. Elevated
452 brain iron has been implicated in several neurodegenerative disorders, including Parkinson's disease,
453 which is characterized by loss of dopaminergic cells (Ward et al., 2014). Thus, the observed findings
454 have implications for better understanding the mechanisms behind DA-related neurodegeneration.

455

456 **Author credit statement**

457 Conceptualisation: A.S. and G.K.; Software, M.A.; Methodology, J.G., G.K., G.P., A.S.; Formal Analysis
458 J.G., G.K., A.S., J.J., F.F., G.P., M.A., and B.A.P.; Visualisation, J.G. Writing – original draft, J.G., G.K.,
459 A.S., F.F.; Writing – Review & Editing G.P., J.J., L.A., B.A.P.

460 **Acknowledgement**

461 We thank the staff of the DyNAMiC project, Frida Magnusson and Emma Simonsson, staff at MRI and
462 PET labs at Umeå University Hospital, and all our participants. We also thank Robin Pedersen for his
463 contribution with the figures.

464 **Conflict of interest**

465 The authors declare no conflict of interest.

466 **Ethics approval**

467 This study was approved by the Regional Ethical board and the local Radiation Safety Committee in
468 Umeå, Sweden.

469 **Data availability statement**

470 Data from the DyNAMiC project cannot be made publicly available due to ethical and legal
471 restrictions. However, access to these original data may be available upon request from the
472 corresponding author.

473

474 **5. References**

475 Andrews-Hanna, J. R., Snyder, A. Z., Vincent, J. L., Lustig, C., Head, D., Raichle, M. E., & Buckner, R. L.
476 (2007). Disruption of Large-Scale Brain Systems in Advanced Aging. *Neuron*, 56(5), 924–935.
477 <https://doi.org/10.1016/j.neuron.2007.10.038>

478 Ashburner, J. (2007). A fast diffeomorphic image registration algorithm. *NeuroImage*, 38(1), 95–113.
479 <https://doi.org/10.1016/j.neuroimage.2007.07.007>

480 Bäckman, L., Ginovart, N., Dixon, R. A., Wahlin, T. B. R., Wahlin, Å., Halldin, C., & Farde, L. (2000).
481 Age-related cognitive deficits mediated by changes in the striatal dopamine system. *American
482 Journal of Psychiatry*, 157(4), 635–637. <https://doi.org/10.1176/appi.ajp.157.4.635>

483 Bäckman, L., Karlsson, S., Fischer, H., Karlsson, P., Brehmer, Y., Rieckmann, A., MacDonald, S. W. S.,
484 Farde, L., & Nyberg, L. (2011). Dopamine D1 receptors and age differences in brain activation
485 during working memory. *Neurobiology of Aging*, 32(10), 1849–1856.
486 <https://doi.org/10.1016/j.neurobiolaging.2009.10.018>

487 Bäckman, L., Nyberg, L., Lindenberger, U., Li, S. C., & Farde, L. (2006). The correlative triad among
488 aging, dopamine, and cognition: Current status and future prospects. *Neuroscience and
489 Biobehavioral Reviews*, 30(6), 791–807. <https://doi.org/10.1016/j.neubiorev.2006.06.005>

490 Cappell, K. A., Gmeindl, L., & Reuter-Lorenz, P. A. (2010). Age differences in prefrontal recruitment
491 during verbal working memory maintenance depend on memory load. *Cortex*, 46(4), 462–473.
492 <https://doi.org/10.1016/j.cortex.2009.11.009>

493 Cass, W. A., Grondin, R., Andersen, A. H., Zhang, Z., Hardy, P. A., Hussey-Andersen, L. K., Rayens, W.
494 S., Gerhardt, G. A., & Gash, D. M. (2007). Iron accumulation in the striatum predicts aging-
495 related decline in motor function in rhesus monkeys. *Neurobiology of Aging*, 28(2), 258–271.
496 <https://doi.org/10.1016/j.neurobiolaging.2005.12.010>

497 Cools, R., & D'Esposito, M. (2011). Inverted-U-Shaped Dopamine Actions on Human Working
498 Memory and Cognitive Control. *Biological Psychiatry*, 69(12), e113–e125.
499 <https://doi.org/https://doi.org/10.1016/j.biopsych.2011.03.028>

500 Daugherty, A. M., Haacke, E. M., & Raz, N. (2015). Striatal iron content predicts its shrinkage and

501 changes in verbal working memory after two years in healthy adults. *Journal of Neuroscience*,
502 35(17), 6731–6743. <https://doi.org/10.1523/JNEUROSCI.4717-14.2015>

503 Daugherty, A. M., & Raz, N. (2015). Appraising the Role of Iron in Brain Aging and Cognition: Promises
504 and Limitations of MRI Methods. *Neuropsychology Review*, 25(3), 272–287.
505 <https://doi.org/10.1007/s11065-015-9292-y>

506 Daugherty, A. M., & Raz, N. (2016). Accumulation of iron in the putamen predicts its shrinkage in
507 healthy older adults: A multi-occasion longitudinal study. *NeuroImage*, 128(1), 11–20.
508 <https://doi.org/10.1016/j.neuroimage.2015.12.045>

509 de Groot, M., Ikram, M. A., Akoudad, S., Krestin, G. P., Hofman, A., Lugt, A., Niessen, W. J., &
510 Vernooij, M. W. (2015). Tract-specific white matter degeneration in aging: The Rotterdam
511 Study. *Alzheimer's & Dementia*, 11(3), 321–330. <https://doi.org/10.1016/j.jalz.2014.06.011>

512 Deistung, A., Schäfer, A., Schweser, F., Biedermann, U., Turner, R., & Reichenbach, J. R. (2013).
513 Toward in vivo histology: A comparison of quantitative susceptibility mapping (QSM) with
514 magnitude-, phase-, and R2*-imaging at ultra-high magnetic field strength. *NeuroImage*, 65,
515 299–314. <https://doi.org/10.1016/j.neuroimage.2012.09.055>

516 Dichtl, S., Haschka, D., Nairz, M., Seifert, M., Volani, C., Lutz, O., & Weiss, G. (2018). Dopamine
517 promotes cellular iron accumulation and oxidative stress responses in macrophages.
518 *Biochemical Pharmacology*, 148, 193–201. <https://doi.org/10.1016/j.bcp.2017.12.001>

519 Efron, B., & Tibshirani, R. (1986). Bootstrap Methods for Standard Errors, Confidence Intervals, and
520 Other Measures of Statistical Accuracy. *Statistical Science*, 1(1), 15–51.
521 <https://doi.org/10.1214/ss/1177013815>

522 Erikson, K. M., Jones, B. C., Hess, E. J., Zhang, Q., & Beard, J. L. (2001). Iron deficiency decreases
523 dopamine D1 and D2 receptors in rat brain. *Pharmacology Biochemistry and Behavior*, 69(3–4),
524 409–418. [https://doi.org/10.1016/S0091-3057\(01\)00563-9](https://doi.org/10.1016/S0091-3057(01)00563-9)

525 Fischer, H., Nyberg, L., Karlsson, S., Karlsson, P., Brehmer, Y., Rieckmann, A., MacDonald, S. W. S.,
526 Farde, L., & Bäckman, L. (2010). Simulating Neurocognitive Aging: Effects of a Dopaminergic
527 Antagonist on Brain Activity During Working Memory. *Biological Psychiatry*, 67(6), 575–580.
528 <https://doi.org/10.1016/j.biopsych.2009.12.013>

529 Fischl, B., Salat, D. H., Busa, E., Albert, M., Dieterich, M., Haselgrove, C., Van Der Kouwe, A., Killiany,
530 R., Kennedy, D., Klaveness, S., Montillo, A., Makris, N., Rosen, B., & Dale, A. M. (2002). Whole
531 brain segmentation: Automated labeling of neuroanatomical structures in the human brain.
532 *Neuron*, 33(3), 341–355. [https://doi.org/10.1016/S0896-6273\(02\)00569-X](https://doi.org/10.1016/S0896-6273(02)00569-X)

533 Fischl, B., Salat, D. H., Van Der Kouwe, A. J. W., Makris, N., Ségonne, F., Quinn, B. T., & Dale, A. M.
534 (2004). Sequence-independent segmentation of magnetic resonance images. *NeuroImage*,
535 23(SUPPL. 1), 69–84. <https://doi.org/10.1016/j.neuroimage.2004.07.016>

536 Fischl, B., Van Der Kouwe, A., Destrieux, C., Halgren, E., Ségonne, F., Salat, D. H., Busa, E., Seidman, L.
537 J., Goldstein, J., Kennedy, D., Caviness, V., Makris, N., Rosen, B., & Dale, A. M. (2004).
538 Automatically Parcellating the Human Cerebral Cortex. *Cerebral Cortex*, 14(1), 11–22.
539 <https://doi.org/10.1093/cercor/bhg087>

540 Garrett, D. D., Kovacevic, N., McIntosh, A. R., & Grady, C. L. (2010). Blood oxygen level-dependent
541 signal variability is more than just noise. *Journal of Neuroscience*, 30(14), 4914–4921.
542 <https://doi.org/10.1523/JNEUROSCI.5166-09.2010>

543 Garzón, B., Sitnikov, R., Bäckman, L., & Kalpouzos, G. (2017). Can transverse relaxation rates in deep
544 gray matter be approximated from functional and T2-weighted FLAIR scans for relative brain

545 iron quantification? *Magnetic Resonance Imaging*, 40, 75–82.
546 <https://doi.org/10.1016/j.mri.2017.04.005>

547 Gorbach, T., Pudas, S., Lundquist, A., Orädd, G., Josefsson, M., Salami, A., de Luna, X., & Nyberg, L.
548 (2017). Longitudinal association between hippocampus atrophy and episodic-memory decline.
549 *Neurobiology of Aging*, 51, 167–176. <https://doi.org/10.1016/j.neurobiolaging.2016.12.002>

550 Grady, C. L., & Garrett, D. D. (2014). Understanding variability in the BOLD signal and why it matters
551 for aging. *Brain Imaging and Behavior*, 8(2), 274–283. <https://doi.org/10.1007/s11682-013-9253-0>

553 Gustavsson, J., Papenberg, G., Falahati, F., Laukka, E. J., & Kalpouzos, G. (2022). Contributions of the
554 Catechol-O-Methyltransferase Val158Met Polymorphism to Changes in Brain Iron Across
555 Adulthood and Their Relationships to Working Memory. *Frontiers in Human Neuroscience*, 16.
556 <https://doi.org/10.3389/fnhum.2022.838228>

557 Haider, L. (2015). Inflammation, Iron, Energy Failure, and Oxidative Stress in the Pathogenesis of
558 Multiple Sclerosis. *Oxidative Medicine and Cellular Longevity*, 2015(3), 1–10.
559 <https://doi.org/10.1155/2015/725370>

560 Hald, A., & Lotharius, J. (2005). Oxidative stress and inflammation in Parkinson's disease: Is there a
561 causal link? *Experimental Neurology*, 193(2), 279–290.
562 <https://doi.org/10.1016/j.expneurol.2005.01.013>

563 Hallgren, B., & Sourander, P. (1958). The Effect of Age on the Non-Haemin Iron in the Human Brain.
564 *Journal of Neurochemistry*, 3(1), 41–51. <https://doi.org/10.1111/j.1471-4159.1958.tb12607.x>

565 Hare, D. J., & Double, K. L. (2016). Iron and dopamine: A toxic couple. *Brain*, 139(4), 1026–1035.
566 <https://doi.org/10.1093/brain/aww022>

567 He, Y., Thong, P. S., Lee, T., Leong, S. ., Mao, B. Y., Dong, F., & Watt, F. (2003). Dopaminergic cell
568 death precedes iron elevation in MPTP-injected monkeys. *Free Radical Biology and Medicine*,
569 35(5), 540–547. <https://doi.org/doi.org/10.1016/j.neurobiolaging.2005.12.010>

570 Innis, R. B., Cunningham, V. J., Delforge, J., Fujita, M., Gjedde, A., Gunn, R. N., Holden, J., Houle, S.,
571 Huang, S.-C., Ichise, M., Iida, H., Ito, H., Kimura, Y., Koeppe, R. A., Knudsen, G. M., Knuuti, J.,
572 Lammertsma, A. A., Laruelle, M., Logan, J., ... Carson, R. E. (2007). Consensus Nomenclature for
573 in vivo Imaging of Reversibly Binding Radioligands. *Journal of Cerebral Blood Flow &*
574 *Metabolism*, 27(9), 1533–1539. <https://doi.org/10.1038/sj.jcbfm.9600493>

575 Johansson, J., Nordin, K., Pedersen, R., Karalija, N., Papenberg, G., Andersson, M., Korkki, S. M.,
576 Riklund, K., Guitart-Masip, M., Rieckmann, A., Bäckman, L., Nyberg, L., & Salami, A. (2022). Bi-
577 phasic patterns of age-related differences in dopamine D1 receptors across the adult lifespan.
578 *BioRxiv*, 1–35. <https://doi.org/10.1101/2022.05.24.493225>

579 Kalpouzos, G. (2018). Brain iron accumulation, and motor and cognitive decline in normal aging.
580 *Revue de Neuropsychologie*, 10(3), 205. <https://doi.org/10.3917/rne.103.0205>

581 Kalpouzos, G., Garzón, B., Sitnikov, R., Heiland, C., Salami, A., Persson, J., & Bäckman, L. (2017).
582 Higher Striatal Iron Concentration is Linked to Frontostriatal Underactivation and Poorer
583 Memory in Normal Aging. *Cerebral Cortex*, 27(6), 3427–3436.
584 <https://doi.org/10.1093/cercor/bhx045>

585 Karrer, T. M., Josef, A. K., Mata, R., Morris, E. D., & Samanez-Larkin, G. R. (2017). Reduced dopamine
586 receptors and transporters but not synthesis capacity in normal aging adults: a meta-analysis.
587 *Neurobiology of Aging*, 57, 36–46. <https://doi.org/10.1016/j.neurobiolaging.2017.05.006>

588 Kaur, D., Yantiri, F., Rajagopalan, S., Kumar, J., Mo, J. Q., Boonplueang, R., Viswanath, V., Jacobs, R.,
589 Yang, L., Beal, M. F., DiMonte, D., Volitakis, I., Ellerby, L., Cherny, R. A., Bush, A. I., & Andersen,
590 J. K. (2003). Genetic or Pharmacological Iron Chelation Prevents MPTP-Induced Neurotoxicity In
591 Vivo. *Neuron*, 37(6), 899–909. [https://doi.org/10.1016/S0896-6273\(03\)00126-0](https://doi.org/10.1016/S0896-6273(03)00126-0)

592 Lammertsma, A. A., & Hume, S. P. (1996). Simplified Reference Tissue Model for PET Receptor
593 Studies. *NeuroImage*, 4(3), 153–158. <https://doi.org/10.1006/nimg.1996.0066>

594 Landau, S. M., Lal, R., O’Neil, J. P., Baker, S., & Jagust, W. J. (2009). Striatal dopamine and working
595 memory. *Cerebral Cortex*, 19(2), 445–454. <https://doi.org/10.1093/cercor/bhn095>

596 Langkammer, C., Schweser, F., Krebs, N., Deistung, A., Goessler, W., Scheurer, E., Sommer, K.,
597 Reishofer, G., Yen, K., Fazekas, F., Ropele, S., & Reichenbach, J. R. (2012). Quantitative
598 susceptibility mapping (QSM) as a means to measure brain iron? A post mortem validation
599 study. *NeuroImage*, 62(3), 1593–1599. <https://doi.org/10.1016/j.neuroimage.2012.05.049>

600 Larsen, B., Olafsson, V., Calabro, F., Laymon, C., Tervo-Clemmens, B., Campbell, E., Minhas, D.,
601 Montez, D., Price, J., & Luna, B. (2020). Maturation of the human striatal dopamine system
602 revealed by PET and quantitative MRI. *Nature Communications*, 11(1), 1–10.
603 <https://doi.org/10.1038/s41467-020-14693-3>

604 Leibovitch, F. S., Black, S. E., Caldwell, C. B., McIntosh, A. R., Ehrlich, L. E., & Szalai, J. P. (1999). Brain
605 SPECT imaging and left hemispatial neglect covaried using partial least squares: The sunnybrook
606 stroke study. *Human Brain Mapping*, 7(4), 244–253. [https://doi.org/10.1002/\(SICI\)1097-0193\(1999\)7:4<244::AID-HBM3>3.0.CO;2-K](https://doi.org/10.1002/(SICI)1097-0193(1999)7:4<244::AID-HBM3>3.0.CO;2-K)

608 Li, W., Wu, B., Batrachenko, A., Bancroft-Wu, V., Morey, R. A., Shashi, V., Langkammer, C., De Bellis,
609 M. D., Ropele, S., Song, A. W., & Liu, C. (2014). Differential developmental trajectories of
610 magnetic susceptibility in human brain gray and white matter over the lifespan. *Human Brain
611 Mapping*, 35(6), 2698–2713. <https://doi.org/10.1002/hbm.22360>

612 Lillig, C. H., Berndt, C., & Holmgren, A. (2008). Glutaredoxin systems. *Biochimica et Biophysica Acta -
613 General Subjects*, 1780(11), 1304–1317. <https://doi.org/10.1016/j.bbagen.2008.06.003>

614 Liu, T., Liu, J., De Rochefort, L., Spincemaille, P., Khalidov, I., Ledoux, J. R., & Wang, Y. (2011).
615 Morphology enabled dipole inversion (MEDI) from a single-angle acquisition: Comparison with
616 COSMOS in human brain imaging. *Magnetic Resonance in Medicine*, 66(3), 777–783.
617 <https://doi.org/10.1002/mrm.22816>

618 Liu, T., Wisnieff, C., Lou, M., Chen, W., Spincemaille, P., & Wang, Y. (2013). Nonlinear formulation of
619 the magnetic field to source relationship for robust quantitative susceptibility mapping.
620 *Magnetic Resonance in Medicine*, 69(2), 467–476. <https://doi.org/10.1002/mrm.24272>

621 Liu, Z., Zhai, X. R., Du, Z. S., Xu, F. F., Huang, Y., Wang, X. Q., Qiu, Y. H., & Peng, Y. P. (2021). Dopamine
622 receptor D2 on CD4+ T cells is protective against neuroinflammation and neurodegeneration in
623 a mouse model of Parkinson’s disease. *Brain, Behavior, and Immunity*, 98(April), 110–121.
624 <https://doi.org/10.1016/j.bbi.2021.08.220>

625 Mattay, V. S., Fera, F., Tessitore, A., Hariri, A. R., Berman, K. F., Das, S., Meyer-Lindenberg, A.,
626 Goldberg, T. E., Callicott, J. H., & Weinberger, D. R. (2006). Neurophysiological correlates of age-
627 related changes in working memory capacity. *Neuroscience Letters*, 392(1–2), 32–37.
628 <https://doi.org/10.1016/j.neulet.2005.09.025>

629 Mazhar, M., Din, A. U., Ali, H., Yang, G., Ren, W., Wang, L., Fan, X., & Yang, S. (2021). Implication of
630 ferroptosis in aging. *Cell Death Discovery*, 7(1), 1–9. <https://doi.org/10.1038/s41420-021-00553-6>

632 McCann, H., Cartwright, H., & Halliday, G. M. (2016). Neuropathology of α -synuclein propagation and
633 braak hypothesis. *Movement Disorders*, 31(2), 152–160. <https://doi.org/10.1002/mds.26421>

634 McIntosh, A. R., Bookstein, F. L., Haxby, J. V., & Grady, C. L. (1996). Spatial pattern analysis of
635 functional brain images using partial least squares. *NeuroImage*, 3(31), 143–157.
636 <https://doi.org/10.1006/nimg.1996.0016>

637 McIntosh, A. R., Chau, W. K., & Protzner, A. B. (2004). Spatiotemporal analysis of event-related fMRI
638 data using partial least squares. *NeuroImage*, 23(2), 764–775.
639 <https://doi.org/10.1016/j.neuroimage.2004.05.018>

640 McIntosh, A. R., & Lobaugh, N. J. (2004). Partial least squares analysis of neuroimaging data:
641 Applications and advances. *NeuroImage*, 23(SUPPL. 1), 250–263.
642 <https://doi.org/10.1016/j.neuroimage.2004.07.020>

643 Mills, E., Dong, X. P., Wang, F., & Xu, H. (2010). Mechanisms of brain iron transport: Insight into
644 neurodegeneration and CNS disorders. *Future Medicinal Chemistry*, 2(1), 51–64.
645 <https://doi.org/10.4155/fmc.09.140>

646 Nordin, K., Gorbach, T., Pedersen, R., Lundmark, V. P., Johansson, J., Andersson, M., McNulty, C.,
647 Riklund, K., Wåhlin, A., Papenberg, G., Kalpouzos, G., Bäckman, L., & Salami, A. (2022).
648 DyNAMiC: A prospective longitudinal study of dopamine and brain connectomes: A new
649 window into cognitive aging. *Journal of Neuroscience Research*, January, 1–25.
650 <https://doi.org/10.1002/jnr.25039>

651 Nyberg, L., Andersson, M., Forsgren, L., Jakobsson-Mo, S., Larsson, A., Marklund, P., Nilsson, L. G.,
652 Riklund, K., & Bäckman, L. (2009). Striatal dopamine D2 binding is related to frontal BOLD
653 response during updating of long-term memory representations. *NeuroImage*, 46(4), 1194–
654 1199. <https://doi.org/10.1016/j.neuroimage.2009.03.035>

655 Nyberg, L., Andersson, M., Kauppi, K., Lundquist, A., Persson, J., Pudas, S., & Nilsson, L.-G. (2014).
656 Age-related and Genetic Modulation of Frontal Cortex Efficiency. *Journal of Cognitive
657 Neuroscience*, 26(4), 746–754. https://doi.org/10.1162/jocn_a_00521

658 Nyberg, L., Dahlin, E., Stigsdotter Neely, A., & Bäckman, L. (2009). Neural correlates of variable
659 working memory load across adult age and skill: Dissociative patterns within the fronto-parietal
660 network: Cognition and Neurosciences. *Scandinavian Journal of Psychology*, 50(1), 41–46.
661 <https://doi.org/10.1111/j.1467-9450.2008.00678.x>

662 Ortega, R., Cloetens, P., Devès, G., Carmona, A., & Bohic, S. (2007). Iron storage within dopamine
663 neurovesicles revealed by chemical nano-imaging. *PLoS ONE*, 2(9).
664 <https://doi.org/10.1371/journal.pone.0000925>

665 Poetini, M. R., Araujo, S. M., Trindade de Paula, M., Bortolotto, V. C., Meichtry, L. B., Polet de
666 Almeida, F., Jesse, C. R., Kunz, S. N., & Prigol, M. (2018). Hesperidin attenuates iron-induced
667 oxidative damage and dopamine depletion in *Drosophila melanogaster* model of Parkinson's
668 disease. *Chemico-Biological Interactions*, 279(September 2017), 177–186.
669 <https://doi.org/10.1016/j.cbi.2017.11.018>

670 Reuter-Lorenz, P. A., & Cappell, K. A. (2008). Neurocognitive aging and the compensation hypothesis.
671 *Current Directions in Psychological Science*, 17(3), 177–182. [https://doi.org/10.1111/j.1467-8721.2008.00570.x](https://doi.org/10.1111/j.1467-
672 8721.2008.00570.x)

673 Rieckmann, A., Karlsson, S., Karlsson, P., Brehmer, Y., Fischer, H., Farde, L., Nyberg, L., & Bäckman, L.
674 (2011). Dopamine D1 receptor associations within and between dopaminergic pathways in
675 younger and elderly adults: Links to cognitive performance. *Cerebral Cortex*, 21(9), 2023–2032.

676 <https://doi.org/10.1093/cercor/bhq266>

677 Rodrigue, K. M., Daugherty, A. M., Foster, C. M., & Kennedy, K. M. (2020). Striatal iron content is
678 linked to reduced fronto-striatal brain function under working memory load. *NeuroImage*,
679 210(October 2019), 116544. <https://doi.org/10.1016/j.neuroimage.2020.116544>

680 Salami, A., Avelar-Pereira, B., Garzón, B., Sitnikov, R., & Kalpouzos, G. (2018). Functional coherence of
681 striatal resting-state networks is modulated by striatal iron content. *NeuroImage*, 183(April),
682 495–503. <https://doi.org/10.1016/j.neuroimage.2018.08.036>

683 Salami, A., Eriksson, J., Kompus, K., Habib, R., Kauppi, K., & Nyberg, L. (2010). Characterizing the
684 neural correlates of modality-specific and modality-independent accessibility and availability
685 signals in memory using partial-least squares. *NeuroImage*, 52(2), 686–698.
686 <https://doi.org/10.1016/j.neuroimage.2010.04.195>

687 Salami, A., Eriksson, J., & Nyberg, L. (2012). Opposing effects of aging on large-scale Brain systems for
688 memory encoding and cognitive control. *Journal of Neuroscience*, 32(31), 10749–10757.
689 <https://doi.org/10.1523/JNEUROSCI.0278-12.2012>

690 Salami, A., Garrett, D. D., Wählén, A., Rieckmann, A., Papenbergs, G., Karalija, N., Jonasson, L.,
691 Andersson, M., Axelsson, J., Johansson, J., Riklund, K., Lövdén, M., Lindenberger, U., Bäckman,
692 L., & Nyberg, L. (2019). Dopamine D 2/3 binding potential modulates neural signatures of
693 working memory in a load-dependent fashion. *Journal of Neuroscience*, 39(3), 537–547.
694 <https://doi.org/10.1523/JNEUROSCI.1493-18.2018>

695 Salami, A., Papenbergs, G., Sitnikov, R., Laukka, E. J., Persson, J., & Kalpouzos, G. (2021). Elevated
696 Neuroinflammation Contributes to the deleterious Impact of Iron Overload on Brain Function in
697 Aging. *NeuroImage*, 230(August 2020), 117792.
698 <https://doi.org/10.1016/j.neuroimage.2021.117792>

699 Salami, A., Rieckmann, A., Fischer, H., & Bäckman, L. (2014). A multivariate analysis of age-related
700 differences in functional networks supporting conflict resolution. *NeuroImage*, 86, 150–163.
701 <https://doi.org/10.1016/j.neuroimage.2013.08.002>

702 Salthouse, T. (2012). Consequences of age-related cognitive declines. *Annual review of psychology*.
703 *Annu Rev Psychol.*, 63, 201–226. <https://doi.org/10.1146/annurev-psych-120710-100328>.Consequences

705 Schneider-Garcés, N. J., Gordon, B. A., Brumback-Peltz, C. R., Shin, E., Lee, Y., Sutton, B. P., Maclin, E.
706 L., Gratton, G., & Fabiani, M. (2010). Span, CRUNCH, and beyond: Working memory capacity
707 and the aging brain. *Journal of Cognitive Neuroscience*, 22(4), 655–669.
708 <https://doi.org/10.1162/jocn.2009.21230>

709 Shao, W., Zhang, S., Tang, M., Zhang, X., Zhou, Z., Yin, Y., Zhou, Q., Huang, Y., Liu, Y., Wawrousek, E.,
710 Chen, T., Li, S., Xu, M., Zhou, J., Hu, G., & Zhou, J. (2013). Suppression of neuroinflammation by
711 astrocytic dopamine D2 receptors via α B-crystallin. *Nature*, 494, 90–94.
712 <https://doi.org/https://doi.org/10.1038/nature11748>

713 Shohamy, D., & Adcock, R. A. (2010). Dopamine and adaptive memory. *Trends in Cognitive Sciences*,
714 14(10), 464–472. <https://doi.org/10.1016/j.tics.2010.08.002>

715 Spence, H., McNeil, C. J., & Waiter, G. D. (2020). The impact of brain iron accumulation on cognition:
716 A systematic review. *PLoS ONE*, 15(10 October). <https://doi.org/10.1371/journal.pone.0240697>

717 Steiger, T. K., Weiskopf, N., & Bunzeck, N. (2016). Iron level and myelin content in the ventral
718 striatum predict memory performance in the aging brain. *Journal of Neuroscience*, 36(12),
719 3552–3558. <https://doi.org/10.1523/JNEUROSCI.3617-15.2016>

720 Straub, S., Schneider, T. M., Emmerich, J., Freitag, M. T., Ziener, C. H., Schlemmer, H. P., Ladd, M. E.,
721 & Laun, F. B. (2017). Suitable reference tissues for quantitative susceptibility mapping of the
722 brain. *Magnetic Resonance in Medicine*, 78(1), 204–214. <https://doi.org/10.1002/mrm.26369>

723 Tabachnick, B., & Fidell, L. (2013). Using Multivariate Statistics. In *Singular Spectrum Analysis* (6th
724 ed.). Pearson. https://doi.org/10.1007/978-1-4757-2514-8_3

725 Unger, E. L., Bianco, L. E., Jones, B. C., Allen, R. P., & Earley, C. J. (2014). Low brain iron effects and
726 reversibility on striatal dopamine dynamics. *Experimental Neurology*, 261, 462–468.
727 <https://doi.org/10.1016/j.expneurol.2014.06.023>

728 Ward, R. J., Zucca, F. A., Duyn, J. H., Crichton, R. R., & Zecca, L. (2014). The role of iron in brain ageing
729 and neurodegenerative disorders. *The Lancet Neurology*, 13(10), 1045–1060.
730 [https://doi.org/10.1016/S1474-4422\(14\)70117-6](https://doi.org/10.1016/S1474-4422(14)70117-6)

731 Xu, W., & Cumming, I. (1999). A region-growing algorithm for InSAR phase unwrapping. *IEEE
732 Transactions on Geoscience and Remote Sensing*, 37(1), 124–134.
733 <https://doi.org/10.1109/36.739143>

734 Yan, Y., Jiang, W., Liu, L., Wang, X., Ding, C., Tian, Z., & Zhou, R. (2015). Dopamine Controls Systemic
735 Inflammation through Inhibition of NLRP3 Inflammasome. *Cell*, 160(1–2), 62–73.
736 <https://doi.org/10.1016/j.cell.2014.11.047>

737 Youdim, M. B. H., Ben-Shachar, D., & Riederer, P. (1993). The possible role of iron in the
738 etiopathology of parkinson's disease. *Movement Disorders*, 8(1), 1–12.
739 <https://doi.org/10.1002/mds.870080102>

740 Zecca, L., Youdim, M., Riederer, P., Connor, J. R., & Crichton, R. R. (2004). Iron, brain ageing and
741 neurodegenerative disorders. *Nature Reviews Neuroscience*, 5(11), 863–873.
742 <https://doi.org/10.1038/nrn1537>

743 Zhu, J., Hu, Z., Han, X., Wang, D., Jiang, Q., Ding, J., Xiao, M., Wang, C., Lu, M., & Hu, G. (2018).
744 Dopamine D2 receptor restricts astrocytic NLRP3 inflammasome activation via enhancing the
745 interaction of β -arrestin2 and NLRP3. *Cell Death & Differentiation*, 25, 2037–2049.
746 <https://doi.org/10.1038/s41418-018-0127-2>

747 Zimmerman, M. E., Brickman, A. M., Paul, R. H., Grieve, S. M., Tate, D. F., Gunstad, J., Cohen, R. A.,
748 Aloia, M. S., Williams, L. M., Clark, C. R., Whitford, T. J., & Gordon, E. (2006). The relationship
749 between frontal gray matter volume and cognition varies across the healthy adult lifespan.
750 *American Journal of Geriatric Psychiatry*, 14(10), 823–833.
751 <https://doi.org/10.1097/01.JGP.0000238502.40963.ac>

752 Zucca, F. A., Segura-Aguilar, J., Ferrari, E., Muñoz, P., Paris, I., Sulzer, D., Sarna, T., Casella, L., & Zecca,
753 L. (2017). Interactions of iron, dopamine and neuromelanin pathways in brain aging and
754 Parkinson's disease. *Progress in Neurobiology*, 155(3), 96–119.
755 <https://doi.org/10.1016/j.pneurobio.2015.09.012>

756